

## Electrical resistivity and seismic refraction tomography to detect buried cavities

Ettore Cardarelli<sup>1\*</sup>, Michele Cercato<sup>1</sup>, Antonio Cerreto<sup>2</sup> and Gerardina Di Filippo<sup>1</sup>

<sup>1</sup>Sapienza University of Rome, DITS, Via Eudossiana 18, 00184 Rome, Italy, and <sup>2</sup>External contractor

Received April 2009, revision accepted October 2009

### ABSTRACT

Near-surface cavities can pose serious hazards to human safety, especially in highly urbanized town centres. The location of subsurface voids, the estimation of their size and the evaluation of the overburden thickness are necessary to assess the risk of collapse.

In this study, electrical resistivity tomography (ERT) and seismic refraction tomography data are integrated in a joint interpretation process for cavity location in the city of Rome.

ERT is a well established and widely employed method for cavity detection. However, additional information provided by seismic refraction tomography is capable of eliminating some potential pitfalls in resistivity data interpretation. We propose that the structure of the cavities defined by ERT can be used as a base to optimize seismic refraction tomography investigations within the framework of a joint interpretation process.

Data integration and the insertion of *a priori* information are key issues for reducing the uncertainties associated with the inversion process and for optimizing both acquisition procedures and computation time.

Herein, the two geophysical methods are tested on both synthetic and real data and the integration of the results is found to be successful in detecting isolated cavities and in assessing their geometrical characteristics. The cavity location inferred by geophysical non-invasive methods has been subsequently confirmed by direct inspection.

**Key words:** Inversion, Tomography, Electrical resistivity survey, Seismic refraction and cavities.

### INTRODUCTION

The sudden collapse of shallow cavities is a serious hazard for human safety and infrastructures. Underground voids develop naturally in karst topographies while cavities such as tombs or catacombs, underground mines, tunnels, buried passageways, etc., are produced by human activities. A geophysical field programme is often the most cost-effective way to obtain subsurface information in either case, especially over large

or highly urbanized areas where the use of drilling may be uneconomical or impractical.

When voids are located in historical centres of towns, the detection of buried cavities is a challenging task for geophysical methods because the logistic limitations may be severe and the noise level caused by the surrounding activities and infrastructures is generally high. In such cases, the selection of the appropriate geophysical methods for cavity detection strongly depends on the geological environment.

Different prospecting techniques have been employed to detect underground voids. Success depends on their ability to reach the target depth with the appropriate resolution

---

\*E-mail: etto.re.cardarelli@uniroma1.it

for each problem. Ground-penetrating radar (GPR) is often employed for mapping shallow cavities (Benson 1995; Chamberlain *et al.* 2000), because it is characterized by rapid data acquisition, dense data coverage and high resolution. Its main drawbacks are limited depth of penetration (especially in cases of conductive overburden) and high sensitivity to cultural noise (generated by power lines, underground networks, etc.). Microgravimetry is also a well-established technique for cavity detection (Butler 1984), although its application in urban environments requires accurate modelling of topography, surrounding buildings and infrastructures (Debeglia and Dupont 2002). Also, it is very sensitive to cultural noise. Electrical resistivity tomography (ERT) is now widely used for underground void detection for both natural (Van Schoor 2002; McDonald and Davies 2003) and archaeological targets (Cardarelli, Fischanger and Piro 2008).

Seismic methods for near-surface characterization are becoming more and more popular because their cost-effectiveness for shallow targets has improved in recent years, as the price of seismic equipment has declined. Synthetic modelling (Sheehan, Doll and Mandell 2005a; Sheehan *et al.* 2005b), experiments on physical-scale models (Grandjean and Leparoux 2004; Grandjean 2006) and field data (Sheehan *et al.* 2005c) have indicated that seismic refraction tomography is a potential tool for cavity detection. Integration of data from different techniques is found to be effective under many circumstances to reduce uncertainty and to link the geophysical evidence to certain subsurface geological features, either for natural (Dobecki and Upchurch 2006) or man-made (Piro, Tsourlos and Tsokas 2001; Cardarelli, Di Filippo and Tuccinardi 2007) cavities.

The experience of our research group in cavity mapping near Rome, Italy, is mainly associated with abandoned pozzolana mines. Pozzolana, also known as pozzolanic ash, is a fine, sandy volcanic ash that reacts with lime in the presence of water to form compounds with properties similar to concrete. The pozzolana-based cement, called *opus caementitium*, was widely used in the Roman age and contributed a great deal to the development of civil engineering. Pozzolana was largely extracted within the municipality of Rome and the underground mines (Fig. 1) constitute quite complex networks of galleries which, after the cessation of mining, were often used as tombs, catacombs or waste dumps. The pozzolana layers are generally located at depths greater than nine metres and hence, mining cavities in them are slightly deeper than usual near-surface archaeological targets. Pozzolana is often interbedded with other types of effusive volcanic formations such as massive tuff or basalt (see, for example, Fig. 11

(a)



(b)



Figure 1 Views of typical galleries excavated to mine pozzolana (after Ventriglia 1971).

in Marra *et al.* 1998). The electrical resistivity of pozzolana is generally low (30–40  $\Omega\text{m}$ , or less) and the average thickness of the pozzolana productive layers within Rome can be as great as 20–30 m. The volcanics interbedded with the pozzolana generally exhibit higher resistivity and elevated seismic speeds of propagation. Thus, if only resistivity data are considered, the stiff and resistive interbedded layers can be mistaken for cavities.

Due to the probable depth of targets and the presence of a conductive background, GPR was not considered for use in this study. In such volcanic formations, the penetration depth of GPR is found to be very limited (Cardarelli, Fischanger and Piro 2008). Microgravimetry was not considered to be a cost-effective investigative tool because of the expense associated with making the data corrections (Debeglia and Dupont

2002) required to adequately resolve surrounding buildings and topography.

ERT was selected for use because it takes advantage of the large resistivity contrast between the conductive pozzolana and the highly resistive air-filled cavities. Seismic refraction

tomography was also selected for use because it can reduce ambiguities in the interpretation process associated with the presence of resistive stiff layers. These methods have been used together in the framework of both sequential inversion (Nath, Shahid and Dewangan 2000) and joint inversion (Gallardo

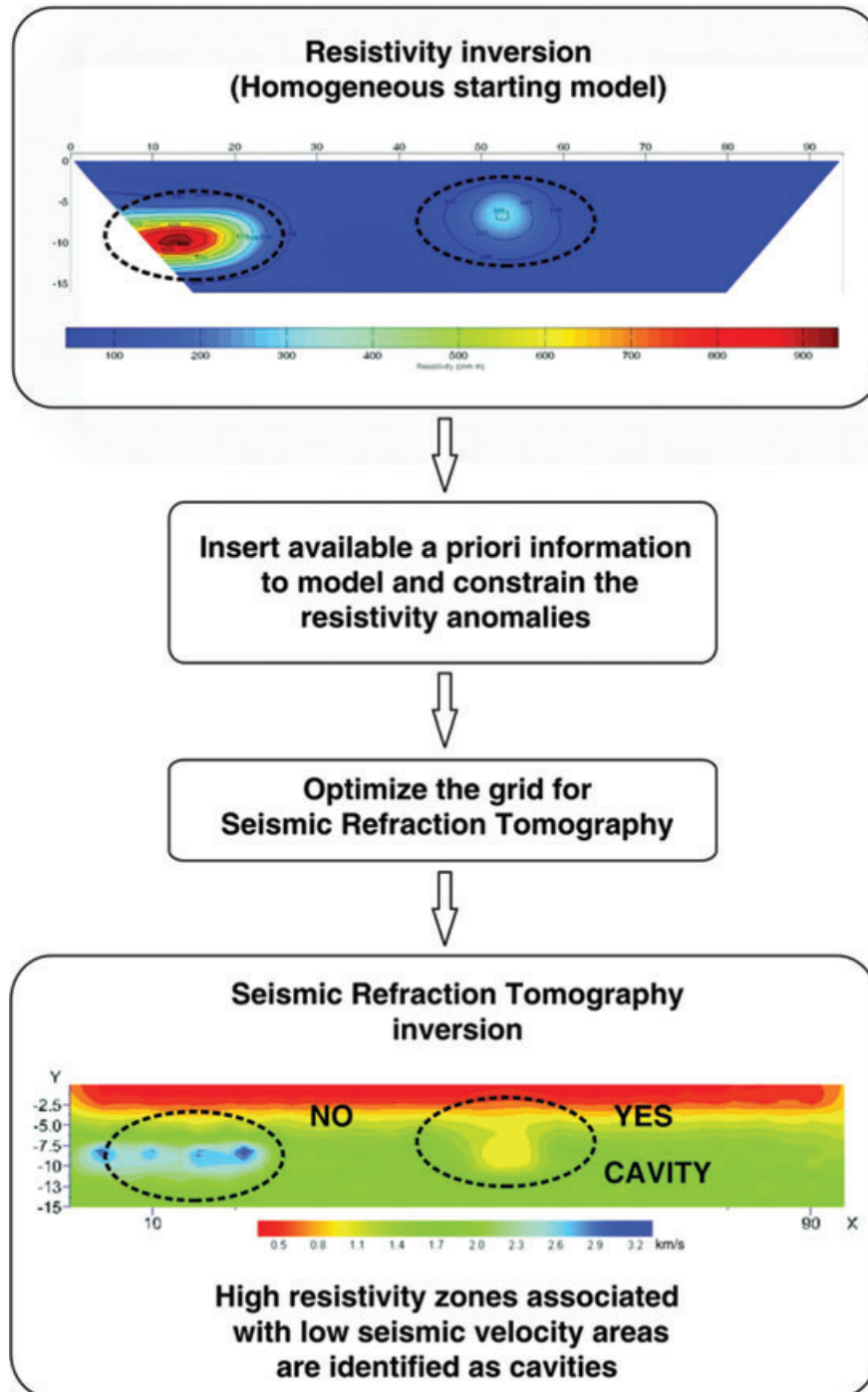
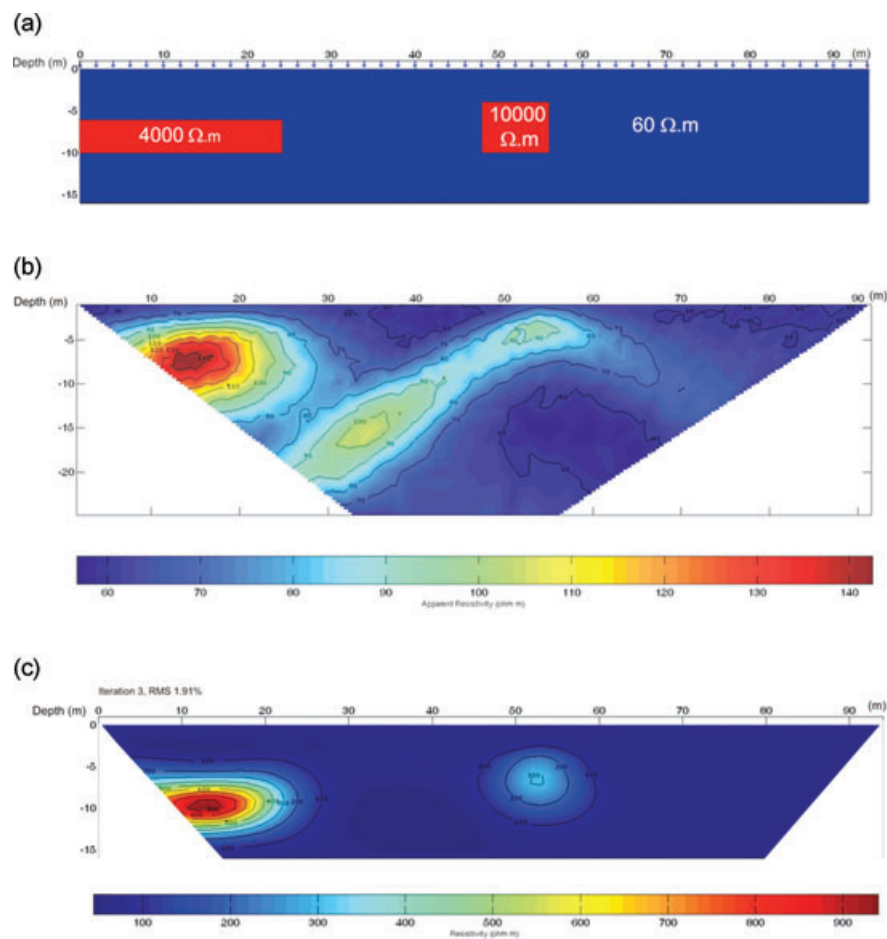


Figure 2 Logical procedure for data integration.

and Meju 2003, 2004; de Nardis, Cardarelli and Dobroka 2005). Joint inversion is usually considered to be advantageous when results obtained by different geophysical methods show a degree of structural similarity. However, there is no such equivalence in the case of cavity detection. In that case, if the cavity is filled with air, ERT indicates high resistivity while seismic refraction tomography indicates low seismic speed (because no waves pass through the void). Thus, if joint inversion of ERT and seismic refraction tomography associates a region of high resistivity with a blurred area of low velocity, it is considered to indicate the presence of an air-filled void (Sheehan *et al.* 2005b). Conversely, if a resistive anomaly located by ERT is linked to a high seismic velocity zone by seismic refraction tomography, the presence of a subsurface void can be excluded. In this way, the integration of data from the two techniques can produce complementary and fruitful results.

## ALGORITHMS AND PROCESSING WORKFLOW FOR DATA INTERPRETATION

The workflow adopted for the joint interpretation of ERT and seismic refraction tomography data, is described in Fig. 2. First, the ERT data are inverted using an initial homogeneous model. This is done using the Versatile algorithm for Electrical Resistivity Data Inversion (VERDI) by Cardarelli and Fischanger (2006), which is based on the formalism of inequality constraints (Kim, Song and Lee 1999). The inequality constraint formulation allows easy introduction of *a priori* information into the inversion process and several options for its insertion are implemented in the software. For example, inserting the standard size and the reference depth of the cavities and setting the background resistivity or imposing limits for the variability of resistivity values tend to refine the interpretation and to better image the shape and dimensions



**Figure 3** Synthetic ERT inversion. a) Model, b) resistivity pseudosection (perturbed with 3% Gaussian noise) and c) inverted model by VERDI (depth range to scale).

of resistivity anomalies, particularly in case of sharp lateral variations (such as in archaeological surveys).

The results from ERT inversion define the average dimension of the resistive anomalies. This has a considerable impact in reducing the cost of the seismic survey. In fact, the number of shots can be reduced and the seismic survey optimized to certain depth targets. ERT results are also used in the seismic refraction tomography inversion to select a grid, generally coarser than the standard grid used in resistivity interpretation, to save computation time and to optimize the seismic inversion process to certain features appearing in the inverted resistivity section.

The seismic refraction tomography algorithm was developed from an already published seismic transmission tomography algorithm (Cardarelli and de Nardis 2001; Cardarelli and Cerreto 2002). The ray-tracing technique is the linear traveltimes interpolation method by Asakawa and Kawanaka (1993) modified to consider anisotropic models (although this option is not used in the present case study). Data inversion is performed by the iterative bi-conjugate gradient algorithm (Press *et al.* 1997). In the implementation presented in this work, the significant change in the seismic refraction tomography programme is that ray-tracing is now performed for surface sources and receivers,

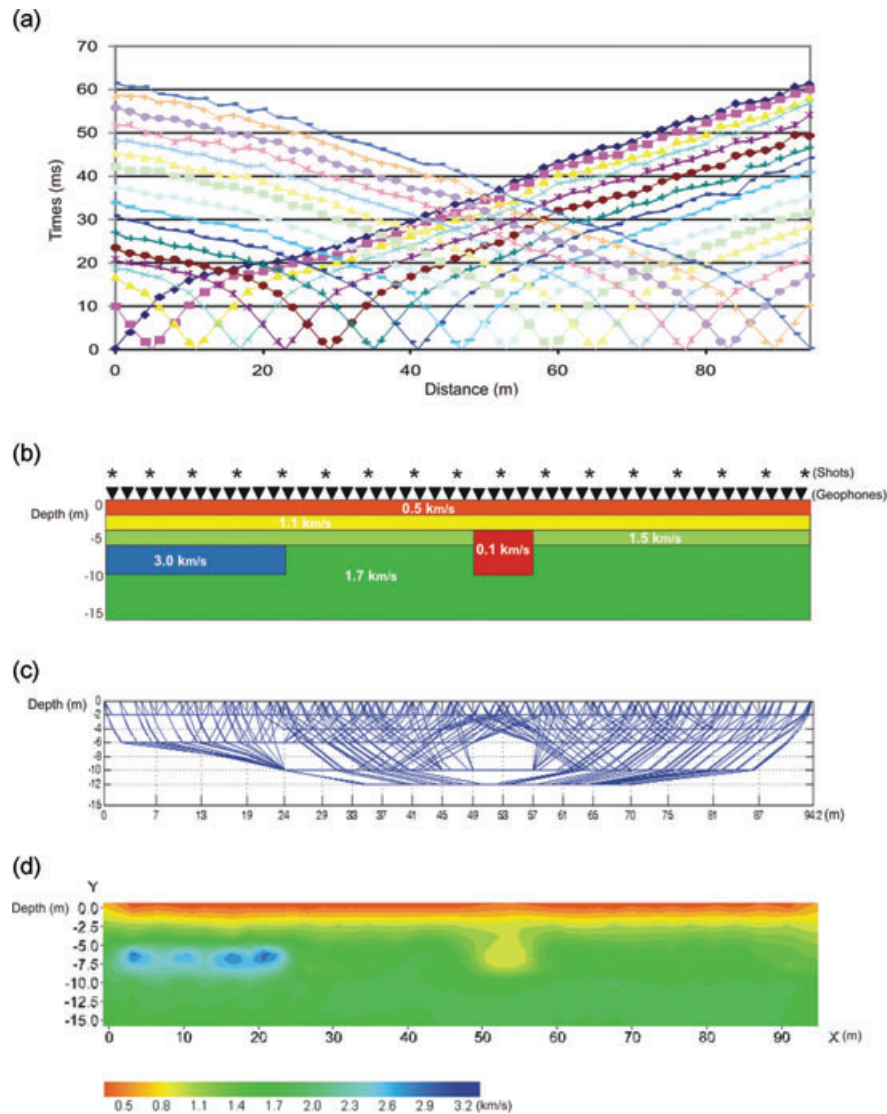


**Figure 4** Synthetic seismic refraction tomography inversion. a) Traveltime curves (3% Gaussian random noise added), b) P-wave velocity model, c) ray-tracing of the inverted model and d) inverted P-wave velocity model (depth range not to scale).

**Table 1** Parameters for field data acquisition

SRT	<ul style="list-style-type: none"> <li>• 48 geophones 4 Hz</li> <li>• Geophones spacing 2 m</li> <li>• 17 shots</li> <li>• Shots distance 6 m</li> <li>• 816 traveltimes</li> <li>• Device – 2 Geode Geometrics</li> <li>• Source hammer 7 kg weight</li> </ul>
ERT	<ul style="list-style-type: none"> <li>• Pole-dipole array (customized sequence)</li> <li>• 48 electrodes</li> <li>• Electrode spacing: 2 m</li> <li>• 1035 apparent resistivity values</li> <li>• Device – Iris Syscal Pro 48 el. 10 channels</li> </ul>

with a simplification in the input interface. Further details about the original algorithm can be found in Cardarelli and Cerreto (2002). By using seismic refraction tomography inversion, the interpreter may identify as cavities only the resistive body associated with low seismic velocity zones, reducing the ambiguities by data integration (Fig. 2).

## SYNTHETIC MODELLING

This section introduces a synthetic example that resembles the geological scenario of the real example that will be presented in the following section. The intention is to illustrate the results that can be obtained by seismic refraction tomography and ERT inversion and to highlight the potential of the integrated procedure. The resistivity synthetic model is displayed in Fig. 3(a) and contains two resistive anomalies: a highly resistive slab of 4000  $\Omega\text{m}$  and a highly resistive square anomaly of 10000  $\Omega\text{m}$ . The background resistivity is set to 60  $\Omega\text{m}$ . The synthetic resistivity pseudosection, obtained by perturbing the theoretical solution of the forward problem with 3% Gaussian noise, is shown in Fig. 3(b). A synthetic data set was computed assuming a pole-dipole array with 48 electrodes at 2 m spacing. Both the smoothness constrained inversion (Cardarelli and Fischanger 2006) and the L1 norm inversion (Olayinka and Yaramanci 2000; Loke, Ackworth and Dahlin 2003) were tested on this synthetic data set. It is known that L1 norm inversion is less sensitive to outliers and tends to produce piecewise constant resistivity models. For this synthetic data set, the inverted models obtained by L1 norm inversion and smoothness constrained inversion were found to be very similar. Hence, only the results of the smoothness constrained inversion are included in the following discussion.

The synthetic data were inverted by VERDI assuming a homogeneous starting model having a resistivity computed as the mean of the synthetic apparent resistivity values in Fig. 3(b).

The inverted model after three iterations is shown in Fig. 3(c). The two high-resistivity anomalies are well recovered by the VERDI inversion as far as their size and depth are concerned. Otherwise, it can be noted that the inversion smoothes the resistivity values of the central square anomaly to about 300  $\Omega\text{m}$ . This occurs because the square anomaly is much smaller than the slab-shaped anomaly. Both anomalies are visible on the electrical inversion results and both could be interpreted as cavities on the basis of the resistivity inversion.

The seismic model (Fig. 4b) is structurally similar to the resistivity model in Fig. 3(a), although the resistive slab-shaped body (on the left) is associated with high P-wave velocity (3.0 km/s) and the square central body with low P-wave velocity (0.1 km/s). Three thin surface layers, whose velocity is increasing with depth from 0.5–1.5 km/s, are added at the surface to produce a more realistic earth model, with heterogeneous surface layers. The synthetic traveltimes in Fig. 4(a) are obtained by adding 3% random Gaussian noise to the noise-free synthetic traveltimes. The ray pattern and the mesh size used for data inversion are shown in Fig. 4(c), while the inverted P-wave velocity section is displayed in Fig. 4(d). The initial model and the mesh design were optimized on the basis of the ERT results; convergence was reached after three external iterations of the biconjugate gradient.

The rms misfit of the inverted P-wave section is equal to 0.63 ms, which represents about 3% of the mean traveltime. This is consistent with the random noise level. The lateral slab-shaped body exhibits a high compressional velocity and therefore cannot be interpreted as an air-filled cavity. The square anomaly, on the other hand, associates high resistivity with a low velocity zone and the presence of a cavity may be deduced with much more confidence.

Thus it is demonstrated that, although both the electrical and seismic methods have the potential to image buried cavities with the required resolution, their integration enables an interpreter to reduce ambiguities in the subsurface reconstruction, especially when the cavities develop within a geological scenario where the presence of stiff resistive formations can not be excluded.

## FIELD SURVEY

In this section, the entire procedure described above, with proper focus on data integration, is applied to a real case study. The site was selected because cavities that exist there are partially accessible and geophysical results can be verified *a posteriori* by direct inspection.

### Geology and site conditions

The site under investigation is a public park located in a highly-populated suburb of Rome. The typical shallow stratigraphy of this area is well-known (see, for example, Fig. 11 in

Marra *et al.* 1998) and, below a surface weathered layer that is generally 1–2 m thick, consists of a succession of volcanic (pyroclastic) formations (mainly pozzolana and tuff) whose thicknesses generally range between 25–35 m. This sequence

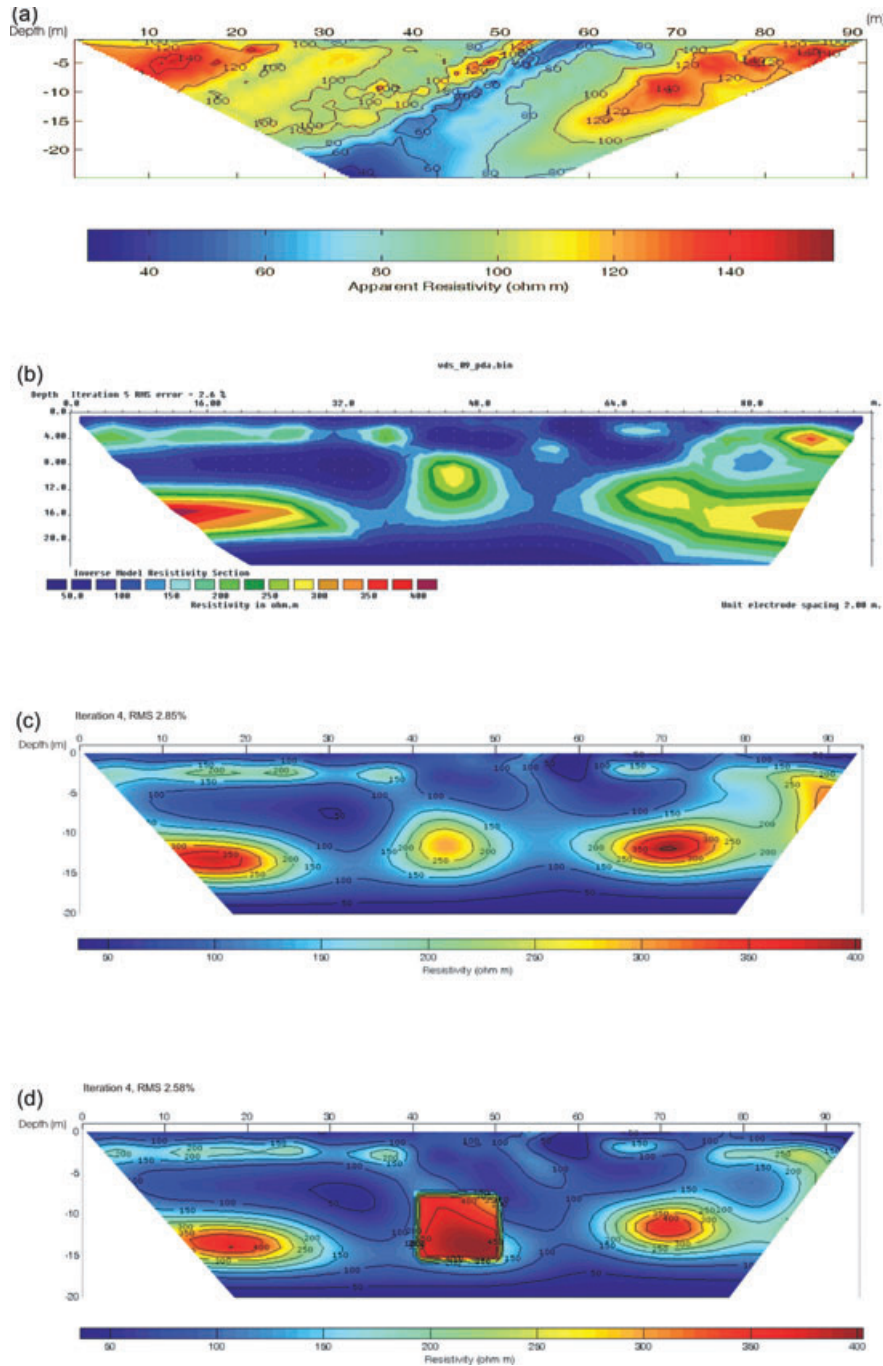


**Figure 5** Real data, ERT inversion. a) Resistivity pseudosection (pole-dipole array), b) inverted section (Res2dinv<sup>©</sup>) using a homogeneous starting model and default inversion parameters, c) inverted section (VERDI) using a homogeneous starting model and d) inverted section (VERDI) using the inversion parameters in Table 2 (depth range not to scale).

overlies alluvial formations of the Tiber River (silt, sand and gravel).

In this area, the water level is documented to be 18 m below ground level (Ventriglia 1971) without noticeable seasonal variations. Cavities are located in the volcanic formations and, as described above, were excavated to mine pozzolana for concrete production. The productive layers are generally located below 9 m depth. The width and height of the underground galleries are both generally 2–5 m. The length of individual galleries can be hundreds of metres (Ventriglia 1971). The size of ERT or seismic refraction tomography anomalies associated with a particular cavity strongly depends on the direction of the profile with respect to the gallery axis. If the profiles are not orthogonal to the gallery axis, the resulting anomaly may have an increased width with respect to the cavity cross-section.

### Field procedure and data interpretation

The first task in the sequential inversion is to isolate individual anomalies that can be successively identified as cavities. The electrical survey was performed using a 2D approach (in-line acquisition) with a pole-dipole array that combined good signal strength and resolution with reasonable depth of investigation. The acquisition parameters for ERT surveys are listed in Table 1 and the results pertaining to one of the electric lines are shown in Fig. 5. First, the apparent resistivity data were inverted using a homogeneous starting model. The field data pseudosection is displayed in Fig. 5(a). In Fig. 5(b,c) the results of the resistivity inversion, starting from an homogeneous model, are displayed for Res2Dinv<sup>®</sup> (Loke and Barker 1996) and VERDI, respectively.

After starting the inversion process with the homogeneous model (Fig. 5b,c), an inhomogeneous model was selected and

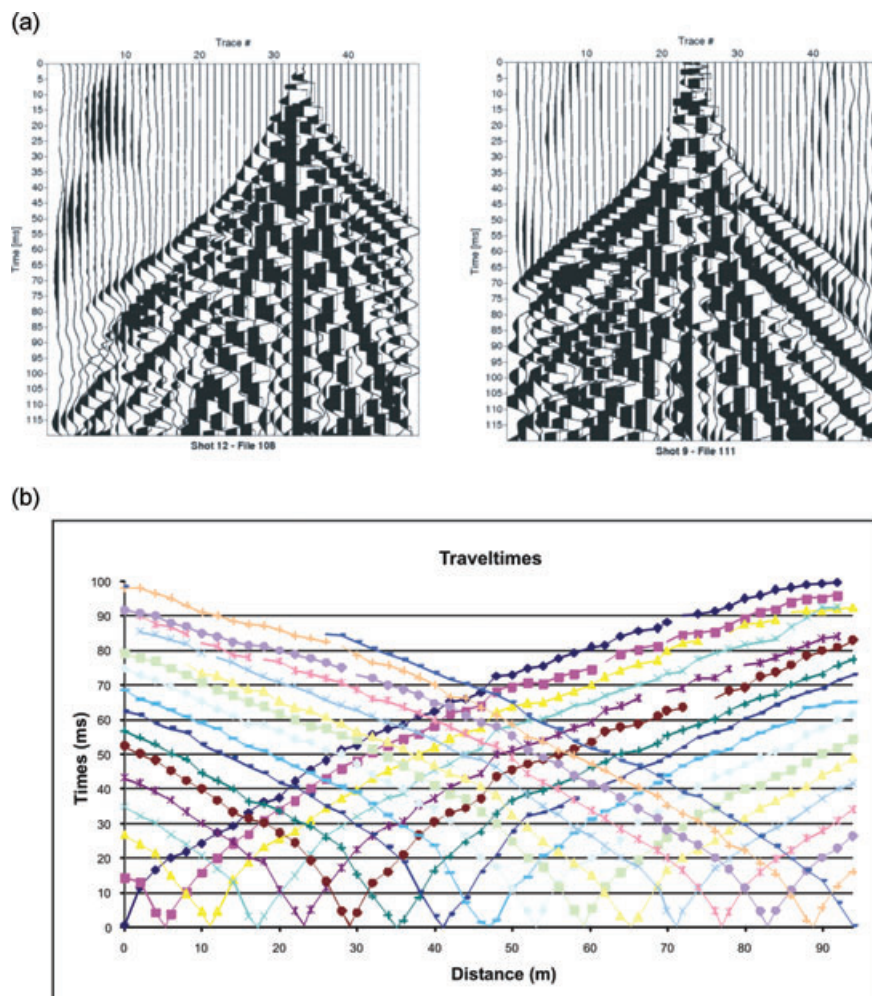
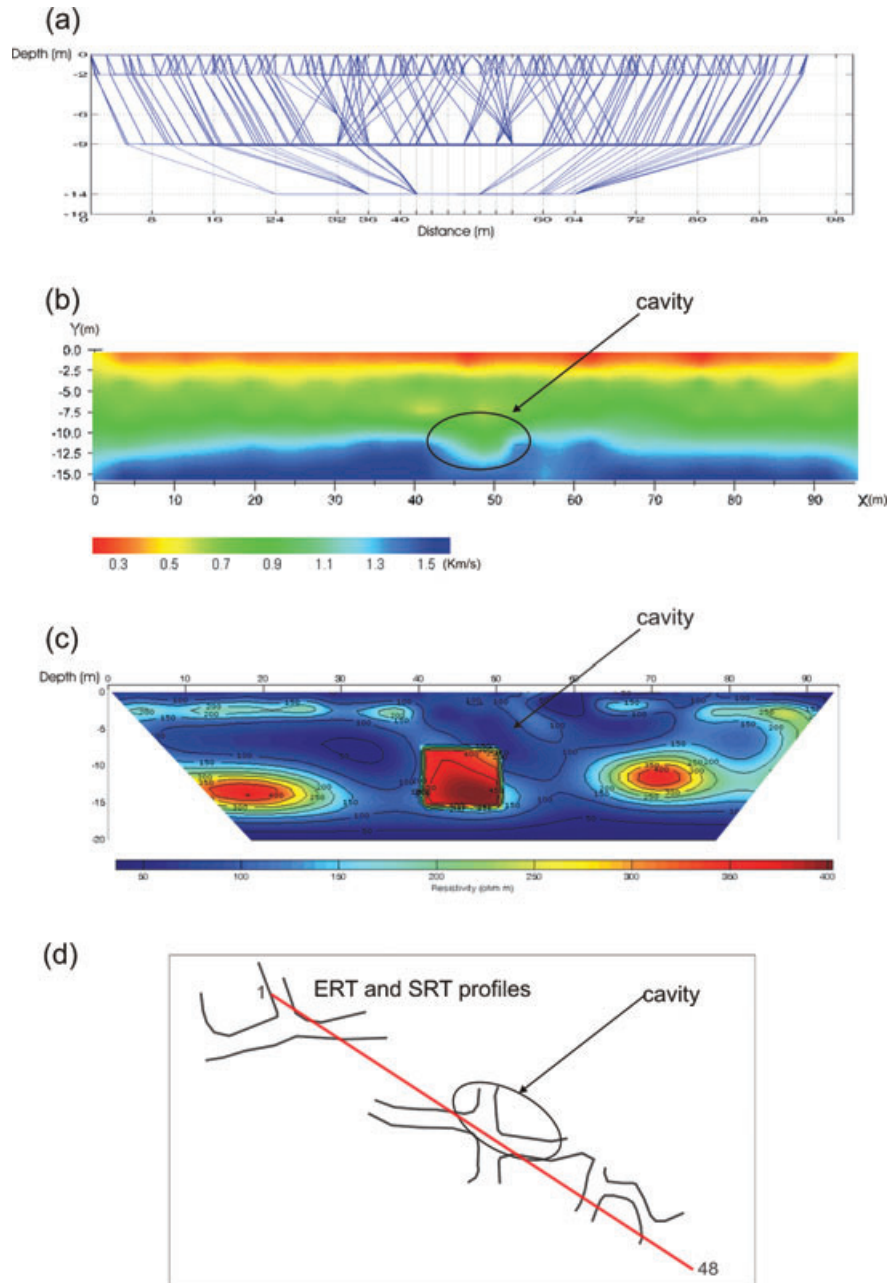


Figure 6 Seismic refraction tomography field data. a) Field seismograms and b) travelttime curves.

data were inverted by VERDI to image the cavity dimension. *A priori* information regarding the usual depth of the cavities (as suggested by the geological study of the area) was merged with the results of the inversions in Fig. 5(b,c). The inhomogeneous starting model included a homogeneous background ( $100 \Omega\text{m}$ ). Inequality constraints were set on a 10 m by 7 m resistive anomaly associated with the central resistive body in

Fig. 5(b,c). Resistivity changes within the anomaly were constrained to be between  $200\text{--}600 \Omega\text{m}$ . The results of this second inversion are shown in Fig. 5(d) and represent an rms misfit of 2.58% at the fourth iteration. Other trials with higher values ( $1000 \Omega\text{m}$  and  $2000 \Omega\text{m}$ ) as the upper boundary of the inequality constraints produced no significant differences in the inverted models.



**Figure 7** a) Raypath for the inverted model, b) inverted P-wave section (the low velocity anomaly is identified as a cavity), c) VERDI inversion as in Fig. 5(d) (depth range is not to scale) and d) sketch map of the floor of the cavity overlapped to ERT and seismic refraction tomography profiles.

Table 2 Parameters for field data inversion

SRT	<ul style="list-style-type: none"> <li>• Number of cells: 95</li> <li>• Sizes: 8 m, 4 m and 2 m.</li> <li>• Thickness: 2 m top, 2° layer 4 m, the 3° 3 m, the 4° 5 m the last 2 m.</li> <li>• Variable damping factor halved at each inner iteration</li> <li>• Four iterations <math>\sigma = 1.3 \text{ ms} \sim 5\%</math></li> </ul>
ERT (VERDI)	<ul style="list-style-type: none"> <li>• Starting model</li> <li>• Dimensions of cavity: 10 m large and 7 m high</li> <li>• Inequality constraints <math>200 &lt; \rho &lt; 1000 \text{ } \Omega\text{m}</math></li> <li>• Background was set to 100 <math>\Omega\text{m}</math></li> <li>• Damping factor halved at each inner iteration</li> </ul>

The resistivity section was integrated by seismic refraction tomography by imposing a seismic line over the ERT line and using the acquisition parameters listed in Table 1. The seismic refraction tomography was performed using 48 geophones and 17 shots for a total of 738 raypaths. The acquisition geometry was selected on the basis of the ERT results to focus on the central resistive body, reducing the number of shots with significant cost savings. The velocity of the bottom layer (1.2 km/s) was evaluated on basis of the traveltime slopes and this value was held fixed during the inversion. Two example shots are shown in Fig. 6(a) and the entire traveltime data set is shown in Fig. 6(b). Data quality proved to be good despite high seismic attenuation in the weathered layer.

During the inversion, constant damping factors were used for each layer, their values being halved at each iteration. The subsoil domain was divided into 95 cells of different sizes as shown in Fig. 7(a). The cell width was decreased toward the centre of the section where data coverage is higher. The thickness of each cell was chosen on the basis of results from the VERDI inversion: the first layer thickness was set to 2 m while the thicknesses of the other layers at increasing depths were assumed to be 4 m, 3 m, 5 m and 2 m, respectively. The inversion was terminated at the fourth external iteration step of the biconjugate gradient. Convergence was reached with an rms misfit equal to 1.3 ms, which represents less than 5% of the mean traveltime. The seismic refraction tomography inversion parameters are listed in Table 2.

## CONCLUSIONS

A cavity between 40–50 m along the  $x$ -axis and 8–15 m deep (Fig. 5d) was detected by two different geophysical techniques.

The VERDI algorithm provided the probable dimensions of the cavity and seismic refraction tomography indicated that the subsoil above the gallery level has low elastic characteristics, the P-wave speed being in the range 0.4–0.6 km/s. Direct inspection confirmed the presence of a 4.5 m wide cavity near the centre of the electrical and seismic sections. The cavity position is indicated in Fig. 7(d) with respect to both the vertical cross-section and the horizontal plan. The cavity width, inferred from the geophysical data to be about 9 m, seems to be overestimated because the electrical profile is not perpendicular to the gallery axis. The cavity depth was properly inferred by the integrated geophysical surveys to be 8–15 m. Therefore the principal conclusion is that the joint interpretation of electrical and seismic tomography successfully located and characterized isolated cavities and their surrounding material.

Two other resistive anomalies, seen in Fig. 7(c) to occur 8–15 m deep, are poorly imaged by the seismic refraction tomography inversion probably due to reduced data coverage and exacerbated by their location beneath an increased thickness of the weathered layer (green layer in Fig. 7b).

Seismic refraction tomography also proved to be useful for determining the elastic characteristics of the materials that overlie the cavity and thereby provide valuable information concerning the risk of a possible vault collapse.

In seismic refraction tomography, a cavity is represented in the inversion by anomalously low seismic speed. However, the speed is not as low as it should be, as also remarked by other authors (Sheehan *et al.* 2005a). This stems from the fact that a cavity has its own resistivity (virtually infinite for air-filled voids) but no seismic rays pass through the void.

When high resistivity and stiff materials are interbedded with conductive layers (containing the cavities), the joint interpretation of ERT and seismic refraction tomography is capable of removing interpretive ambiguity concerning cavity identification while at the same time reducing the cost associated to the seismic investigations. In fact, the ERT results are of great help in optimizing the seismic investigations, focusing the interpretation on specific targets (with many savings in the field operation and interpretation time). Moreover, cavity identification by the associating resistive anomalies with regions of low seismic speed removes some potential resistivity inversion pitfalls where the probable presence of resistive layers has to be taken into account in data interpretation.

## ACKNOWLEDGEMENTS

Prof. Francesca Bozzano and Dr Gianluca Bianchi Fasani ('Sapienza' University of Rome, CERI) are thanked for the

geological investigation and for providing the final map of cavity locations. The authors are grateful to Francesco Pugliese, Marco Alonzi and Giorgio De Donno of 'Sapienza' University of Rome for contributing to the field data acquisition and to Prof. Luis A. Gallardo and to an anonymous reviewer for the insightful suggestions and constructive criticism that greatly improved the paper. Finally, the authors are indebted to Prof. Tom McGee (University of Mississippi, CMRET) for his language editing of the final version of the manuscript.

## REFERENCES

- Asakawa E. and Kawanaka T. 1993. Seismic ray tracing using linear travel time interpolation. *Geophysical Prospecting* **41**, 99–111.
- Benson A.K. 1995. Applications of ground penetrating radar in assessing some geological hazards: Examples of groundwater contamination, faults, cavities. *Journal of Applied Geophysics* **33**, 177–193.
- Butler D.K. 1984. Microgravimetric and gravity gradient techniques for the detection of subsurface cavities. *Geophysics* **49**, 1084–1096.
- Cardarelli E. and Cerreto A. 2002. Ray tracing in elliptical anisotropic media using linear travel-time seismic interpolation (LTI) method applied to traveltimes seismic tomography. *Geophysical Prospecting* **50**, 55–72.
- Cardarelli E., Di Filippo G. and Tuccinardi E. 2007. Electrical resistivity tomography to detect buried cavity in Rome (A case study). *Near Surface Geophysics* **5**, 387–392.
- Cardarelli E. and Fischanger F. 2006. 2D data modelling by electrical resistivity tomography for complex subsurface geology. *Geophysical Prospecting* **54**, 121–134.
- Cardarelli E., Fischanger F. and Piro S. 2008. Integrated geophysical survey to detect buried structures for archaeological prospecting. A case-history at Sabine Necropolis (Rome, Italy). *Near Surface Geophysics* **6**, 15–20.
- Cardarelli E. and de Nardis R. 2001. Seismic refraction, isotropic and anisotropic seismic tomography on an ancient monument. *Geophysical Prospecting* **49**, 228–240.
- Chamberlain A.T., Sellers W., Proctor C. and Coard R. 2000. Cave detection in limestone using ground penetrating radar. *Journal of Archaeological Science* **27**, 957–964.
- Debeglia N. and Dupont F. 2002. Some critical factors for engineering and environmental microgravity investigations. *Journal of Applied Geophysics* **50**, 435–454.
- Dobecki T.L. and Upchurch S.B. 2006. Geophysical applications to detect sinkholes and ground subsidence. *The Leading Edge* **25**, 336–341.
- Gallardo L.A. and Meju M.A. 2003. Characterization of heterogeneous near-surface materials by joint 2D inversion of dc resistivity and seismic data. *Geophysical Research Letters* **30**, 1658.
- Gallardo L.A. and Meju M.A. 2004. Characterization of heterogeneous near-surface materials by joint 2D inversion of dc resistivity and seismic data. *Journal of Geophysical Research* **109**, B03311.
- Grandjean G. 2006. Imaging subsurface objects by seismic P-wave tomography: Numerical and experimental validation. *Near Surface Geophysics* **4**, 279–287.
- Grandjean G. and Leparoux D. 2004. The potential of seismic methods for detecting cavities and buried objects: Experimentation at a test site. *Journal of Applied Geophysics* **56**, 93–106.
- Kim H.J., Song Y. and Lee K.H. 1999. Inequality constraint in least-squares inversion of geophysical data. *Earth Planets Space* **51**, 255–259.
- Loke M.H., Acworth I. and Dahlin T. 2003. A comparison of smooth and blocky inversion methods in 2D electrical imaging surveys. *Exploration Geophysics* **34**, 182–187.
- Loke M.H. and Barker R.D. 1996. Rapid least-squares inversion of apparent resistivity pseudosections by a quasi-Newton method. *Geophysical Prospecting* **44**, 131–152.
- Marra F., Rosa C., De Rita D. and Funicello R. 1998. Stratigraphic and tectonic features of the Middle Pleistocene sedimentary and volcanic deposits in the area of Rome (Italy). *Quaternary International* **47–48**, 51–63.
- McDonald R. and Davies R. 2003. Detection of sinkholes using 2D electrical resistivity imaging. *First Break* **21**, 32–35.
- de Nardis R., Cardarelli E. and Dobroka M. 2005. Quasi-2D hybrid joint inversion of seismic and geoelectric data. *Geophysical Prospecting* **53**, 705–716.
- Nath S.K., Shahid S. and Dewangan P. 2000. SEISRES, a Visual C++ program for the sequential inversion of seismic refraction and geoelectric data. *Computers & Geosciences* **26**, 177–200.
- Olayinka A.I. and Yaramanci U. 2000. Use of block inversion in the 2-D interpretation of apparent resistivity data and its comparison with smooth inversion. *Journal of Applied Geophysics* **45**, 63–81.
- Piro S., Tsourlos P.I. and Tsokas G.N. 2001. Cavity detection employing advanced geophysical techniques: A case study. *European Journal of Environmental and Engineering Geophysics* **6**, 3–31.
- Press W.H., Teukolsky S.A., Vetterling W.T. and Flannery B.P. 1997. *Numerical Recipes in C*. Cambridge University Press. ISBN 0521431085.
- Sheehan J.R., Doll W.E. and Mandell W.A. 2005a. An evaluation of methods and available software for seismic refraction tomography analysis. *Journal of Environmental and Engineering Geophysics* **10**, 21–34.
- Sheehan J.R., Doll W.E., Mandell W.A. and Watson D. 2005b. Cavity detection using seismic refraction tomography: Can it be done? Near Surface meeting, Palermo, Italy, Expanded Abstracts, C004.
- Sheehan J.R., Doll W.E., Watson D. and Mandell W.A. 2005c. Application of Seismic Refraction Tomography to karst cavities. US Geological Survey Karst Interest Group Proceedings, Rapid City, South Dakota, 12–15 September 2005, 29–38.
- Van Schoor M. 2002. Detection of sinkholes using 2D electrical resistivity imaging. *Journal of Applied Geophysics* **50**, 393–399.
- Ventriglia U. 1971. *La geologia della città di Roma*. Amministrazione Provinciale di Roma, Rome (in Italian).